LETTER

doi:10.1038/nature14858

Allosteric receptor activation by the plant peptide hormone phytosulfokine

Jizong Wang[1]*, Hongju Li[2]*, Zhifu Han[1], Heqiao Zhang[1], Tong Wang[2], Guangzhong Lin[1], Junbiao Chang[3], Weicai Yang[2] & Jijie Chai[1]

Phytosulfokine (PSK) is a disulfated pentapeptide that has a ubiquitous role in plant growth and development[1,2]. PSK is perceived by its receptor PSKR[3,4], a leucine-rich repeat receptor kinase (LRR-RK). The mechanisms underlying the recognition of PSK, the activation of PSKR and the identity of the components downstream of the initial binding remain elusive. Here we report the crystal structures of the extracellular LRR domain of PSKR in free, PSK- and co-receptor-bound forms. The structures reveal that PSK interacts mainly with a β-strand from the island domain of PSKR, forming an anti-β-sheet. The two sulfate moieties of PSK interact directly with PSKR, sensitizing PSKR recognition of PSK. Supported by biochemical, structural and genetic evidence, PSK binding enhances PSKR heterodimerization with the somatic embryogenesis receptor-like kinases (SERKs). However, PSK is not directly involved in PSKR–SERK interaction but stabilizes PSKR island domain for recruitment of a SERK. Our data reveal the structural basis for PSKR recognition of PSK and allosteric activation of PSKR by PSK, opening up new avenues for the design of PSKR-specific small molecules.

Peptide signalling has critical roles in regulating plant physiology[1]. Phytosulfokine (PSK)[5] is a secreted disulfated pentapeptide (Tyr(SO_3H)-Ile-Tyr(SO_3H)-Thr-Gln) that has ubiquitous roles in plant growth and development[2]. PSK matures through proteolytic cleavage of its precursor proteins[6] with post-translational sulfation[7] for its full activity[8,9]. PSK receptor was first identified in *Daucus carota* (carrot)[3] and the corresponding gene *DcPSKR* is conserved among plants including *Arabidopsis* that encodes two *PSKR* orthologues, *PSKR1* (ref. 4) and *PSKR2* (ref. 10), but PSK perception largely relies on PSKR1 (ref. 10).

DcPSKR and PSKR1/2 (PSKRs) belong to the large family of leucine-rich repeat receptor kinases (LRR-RKs) with an extracellular LRR domain and a cytoplasmic kinase domain (KD)[11]. The extracellular domains of the three LRR-RKs contain 21 LRRs with an island domain (ID) required for PSK perception[3,10]. PSK binding induces signalling mediated by Ca^{2+}/CaM binding and the kinase activity of PSKR1 (ref. 12), suggesting that ligand binding activates the $PSKR1^{KD}$, as observed in the well-studied RKs such as flagellin insensitive 2 (FLS2) and brassinosteroid insensitive 1 (BRI1)[13]. Signalling mediated by the latter two receptor kinases requires ligand-enhanced heterodimerization with the LRR-RK BAK1 (ref. 14), a member of somatic embryogenesis receptor-like kinases (SERKs) that generally act as a co-receptor with other LRR-RKs[15].

We first solved the crystal structures of the PSK–$PSKR1^{LRR}$ (Fig. 1a and Extended Data Table 1) and PSK–$DcPSKR^{LRR}$ (Extended Data Fig. 1a and Extended Data Table 1) complexes. PSK adopts a β-strand conformation, forming an anti-parallel β-sheet with the $PSKR1^{ID}$ (Fig. 1a). Besides the hydrogen bonds within the β-sheet (Fig. 1b), $PSKR1^{Ser370}$, $PSKR1^{Ser372}$, $PSKR1^{Thr398}$ and $PSKR1^{Asp445}$ from the inner side of the helical structure also form hydrogen bonds with the main chain of PSK (Fig. 1c). Additionally, $PSKR1^{Arg300}$ and $PSKR1^{Asn346}$ form hydrogen bonds with the free carboxyl group of PSK^{Gln5} (Fig. 1c), whereas $PSKR1^{Phe506}$ tightly packs against PSK^{Gln5} and PSK^{Tyr3}. The two sulfate moieties contribute to PSK–$PSKR1^{LRR}$ interactions via both hydrogen bonds involving $PSKR1^{Lys508}$ and $PSKR1^{Asn424}$ and van der Waals packing involving $PSKR1^{Leu399}$, $PSKR1^{Trp448}$ and $PSKR1^{Lys508}$ (Fig. 1b, c). The PSK-interacting residues of PSKR1 are highly conserved in DcPSKR (Extended Data Fig. 1b, c) and PSKR2 (Extended Data Fig. 1d), suggesting that the three PSKRs are conserved in PSK recognition. Indeed, the structure of PSK–$DcPSKR^{LRR}$ is almost identical to that of PSK–$PSKR1^{LRR}$ (Fig. 1d) with a r.m.s.d. (root mean square deviation) of 1.45 Å. Further supporting the sulfate group-mediated PSK–$DcPSKR^{LRR}$ interactions, microscale thermophoresis (MST) showed that PSK displayed a higher binding affinity with $DcPSKR^{LRR}$ than the desulfated PSK (dPSK) (Extended Data Fig. 2a), agreeing with the observation that dPSK promotes root elongation of *Arabidopsis* plants but with a lower activity than PSK[8]. Previous studies using microsomal fractions derived from cells showed that PSK–PSKR interaction displayed a dissociation constant of 4.2 nM in carrot[3] and 7.7 nM in *Arabidopsis*[4], approximately 200–370 times stronger than the affinity measured between $DcPSKR^{LRR}$ and PSK by MST. The precise reason for the affinity difference between cell-based and *in vitro* quantification assays is unclear, but it is possible that interactions between transmembrane or cytoplasmic domains within the cellular context provide an environment more favourable for PSK interaction with its receptor. Assays using MST also confirmed the important role of the critical $DcPSKR^{LRR}$ residues (Extended Data Fig. 1b, c) in PSK recognition, as their mutations compromised PSK–$DcPSKR^{LRR}$ association, albeit to varying degrees (Extended Data Fig. 2b).

As observed previously[8], the *pskr1-3 Arabidopsis* mutants displayed a shortened root phenotype (Fig. 1e). The phenotype was fully complemented by wild-type (WT) *PSKR1* and the chimaeric *PSKR1* carrying $DcPSKR^{LRR}$ and the transmembrane domain and KD of PSKR1, and almost fully complemented by *DcPSKR* (Fig. 1e), but not by the *PSKR1* constructs carrying mutations of the residues critical for PSK–PSKR1 interaction (Fig. 1b, c, e). Furthermore, plants carrying the single *PSKR1* mutants were less responsive to PSK than the WT plants (Extended Data Fig. 2c).

PSK binding induced no oligomerization of $PSKR1^{LRR}$ or $DcPSKR^{LRR}$ (Extended Data Fig. 3), suggesting that a co-receptor is required for their activation based on the dimerization model[14]. PSKR1/2 and DcPSKR belong to the same family of LRR-RKs as BRI1 (ref. 11) that utilizes a SERK member as its co-receptor[13]. Moreover, PSK promotes somatic embryogenesis[16], a marker of which is DcSERK[17]. These data prompted us to hypothesize that a SERK member functions as a co-receptor with PSKRs. Indeed, gel filtration showed that PSK induced the formation of a complex between $PSKR1^{LRR}$ and $SERK1/2/BAK1^{LRR}$ (Fig. 2a and Extended Data Fig. 4a, b). $PSKR1^{LRR}$–$SERK1^{LRR}$ (Fig. 2a)

[1]Ministry of Education Key Laboratory of Protein Science, Center for Structural Biology, School of Life Sciences, Tsinghua-Peking Joint Center for Life Sciences, Tsinghua University, Beijing 100084, China. [2]State Key Laboratory of Molecular Developmental Biology, Institute of Genetics and Developmental Biology, Chinese Academy of Sciences, Beijing 100101, China. [3]School of Chemistry and Molecular Engineering, Zhengzhou University, Zhengzhou 450001, China.
*These authors contributed equally to this work.

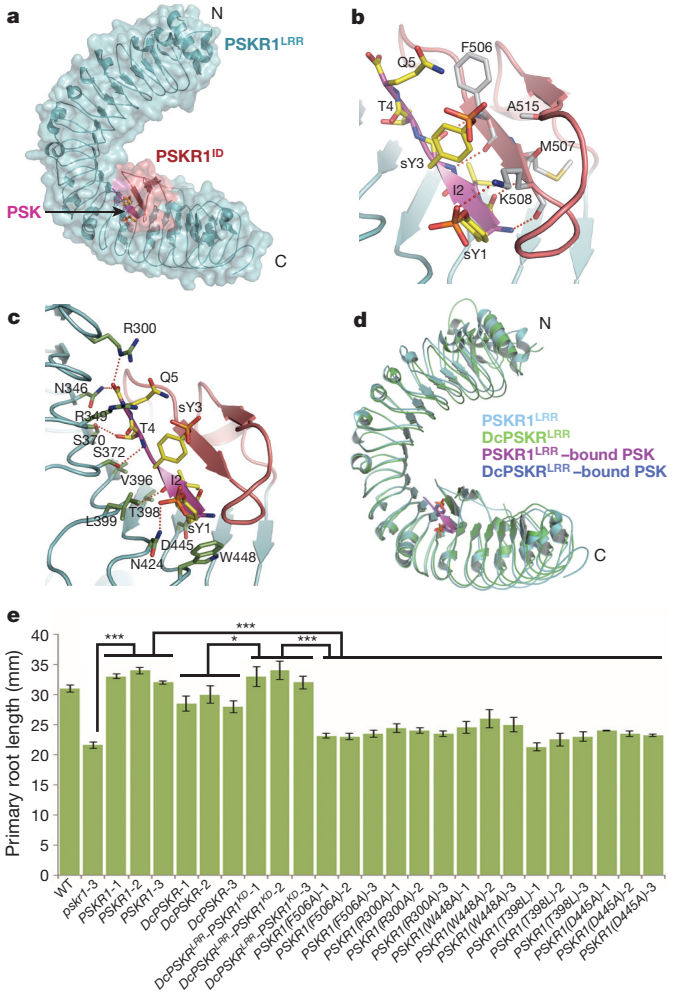

Figure 1 | Recognition mechanism of PSK by PSKR1^{LRR}. **a**, Overall structure of PSK–PSKR1^{LRR} complex. Arrow indicates the position of PSK. ID, island domain. **b**, Detailed interactions of PSK (purple) with the ID (salmon) of PSKR1^{LRR}. sY, sulfated tyrosine. **c**, Detailed interactions of PSK with the inner surface (cyan) of PSKR1^{LRR}. **d**, Structural comparison of PSK–PSKR1$^{LRR(31–631)}$ and PSK–DcPSKR$^{LRR(29–640)}$. **e**, Reducing PSK–PSKR1^{LRR} interaction compromises *PSKR1* to complement the shortened root phenotype of *pskr1-3* mutants. Average (±s.e.m.) primary root lengths of seedlings were determined in three independent experiments. Three independent overexpression lines (represented by -1, -2 and -3) per genotype were analysed ($n = 30$ for each line, $^*P < 0.05$, $^{***}P < 0.001$, Student's *t*-test).

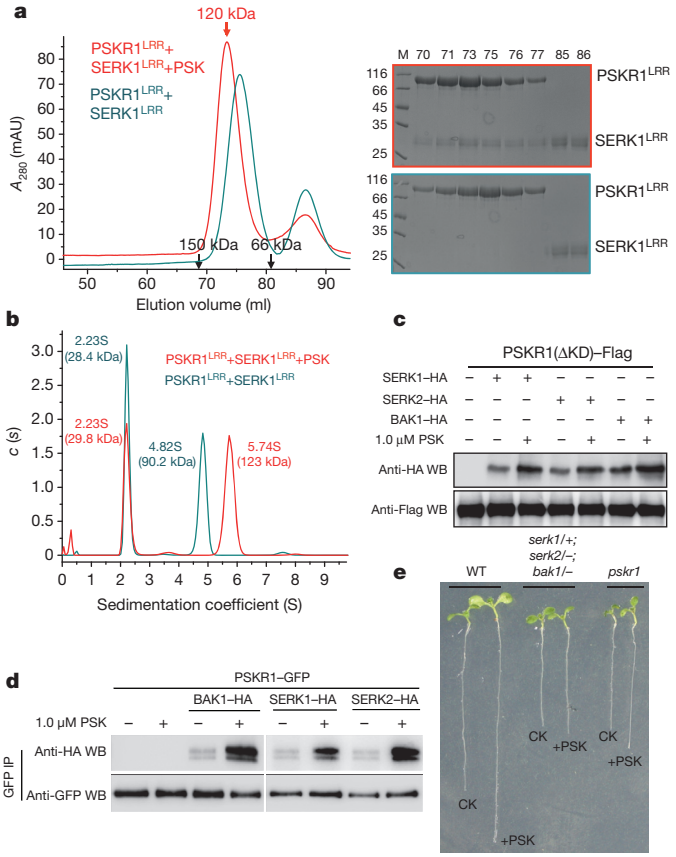

Figure 2 | PSK promotes PSKR–SERK heterodimerization. **a**, PSK induces PSKR1^{LRR}–SERK1^{LRR} heterodimerization. Left, superposition of the gel filtration chromatograms of the PSKR1^{LRR} and SERK1^{LRR} proteins. The red and black arrows indicate the elution positions of PSK–PSKR1^{LRR}–SERK1^{LRR} and molecular weight markers, respectively. mAU, micro-ultraviolet absorbance at 280 nm. Right, Coomassie blue staining of the peak fractions shown on the left following SDS–PAGE. M, molecular weight ladder (kDa). **b**, PSK induces a monomeric PSK–PSKR1^{LRR}–SERK1^{LRR} complex in sedimentation-velocity analytical ultracentrifugation. The peak sedimentation coefficients and the calculated molecular weights for the proteins indicated are shown. **c**, PSK promotes PSKR1–SERK interaction in *Arabidopsis* protoplasts. Flag-tagged PSKR1(ΔKD) and HA-tagged SERK1/2/BAK1 were co-expressed in WT *Arabidopsis* protoplasts, and their interactions were detected by co-immunoprecipitation (Co-IP). Each assay was repeated three times. Full blots are shown in Supplementary Data. **d**, PSK promotes PSKR1–SERK interaction *in planta*. Crude protein extracts from the treated and untreated plants overexpressing green fluorescent protein-conjugated PSKR1 (PSKR1–GFP) and SERK1/2/BAK1–HA were used for Co-IP experiments. Each assay was repeated three times. Full blots are shown in Supplementary Data. **e**, The *serk1/+;serk2/−;bak1/−* triple mutants are less sensitive to PSK in root growth. Wild-type or mutant *Arabidopsis* plants were grown for 10 days on plates with (+PSK) or without (CK) 1.0 μM PSK. The image is representative of ten plants for each genotype.

or DcPSKR^{LRR}–SERK1/2^{LRR} (Extended Data Fig. 4c, d) was heterodimeric in solution as indicated by gel filtration. Further supporting the gel filtration data, sedimentation-velocity analytical ultracentrifugation showed that PSKR1^{LRR} formed a PSK-induced heterodimer with SERK1/2^{LRR} or BAK1^{LRR} (Fig. 2b and Extended Data Fig. 5).

Co-expression of full length Flag-conjugated PSKR1 (PSKR1–Flag) with haemagglutinin (HA)-conjugated SERKs resulted in rupture of *Arabidopsis* protoplasts quickly. We therefore used a KD truncated PSKR1 (PSKR1(ΔKD))–Flag and SERK1/SERK2/BAK1–HA for co-expression in protoplasts. Co-immunoprecipitation (Co-IP) assays showed that PSKR1(ΔKD) interacted with SERK1, SERK2 or BAK1 in protoplasts even in the absence of PSK (Fig. 2c), probably resulting from the endogenous PSK or their constitutive interaction, as observed for the BRI1–BAK1 interaction[18]. Importantly, the PSKR1(ΔKD)–SERK interactions were substantially increased in the PSK-treated protoplasts (Fig. 2c). Similar results were also obtained in *Arabidopsis* co-expressing PSKR1 and BAK1, SERK1 or SERK2 (Fig. 2d). Further supporting these results, the triple *serk1/+;serk2/−;bak1/−* mutant plants (where *serk1* is heterozygote *serk2* and *bak1* are homozygote) had shortened roots much less sensitive to PSK than the wild type (WT) plants, phenocopying the *pskr1-3* mutants (Fig. 2e). Only slightly shorter roots were observed in the single or double knockout plants (Extended Data Fig. 6a, b) that were still PSK-sensitive (Extended Data Fig. 6c), suggesting functional redundancy of SERKs in PSK-induced plant growth. It should be noted that the plant sensitivity to PSK was significantly reduced by inhibition of brassinosteroid-induced signalling[19] in which BAK1 and other SERK members play essential roles[13].

We then solved the crystal structures of the PSK–PSKR1^{LRR}–SERK1^{LRR} (Fig. 3a and Extended Data Table 1) and PSK–DcPSKR^{LRR}–SERK2^{LRR} (Extended Data Fig. 7a and Extended Data Table 1) complexes. The structures of PSKR1^{LRR} and DcPSKR^{LRR}

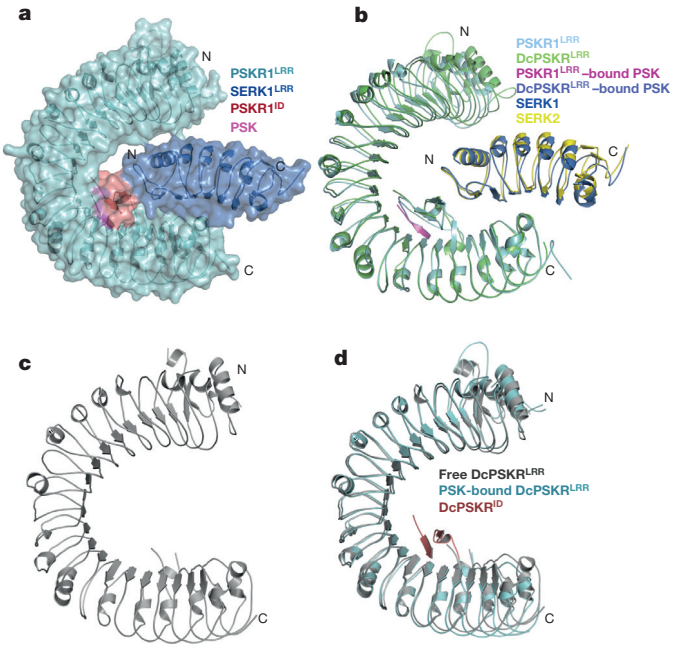

Figure 3 | PSK stabilizes the PSKR^{ID} for interaction with SERKs^{LRR}. **a**, Overall structure of the PSK–PSKR1^{LRR}–SERK1^{LRR} complex. **b**, Structural comparison of PSK–PSKR1$^{LRR(31–638)}$–SERK1^{LRR} and PSK–DcPSKR$^{LRR(29–647)}$–SERK2^{LRR}. **c**, Overall structure of the free DcPSKR^{LRR}. **d**, PSK binding stabilizes the DcPSKR^{ID}. Shown is the structural alignment of free DcPSKR^{LRR} (residues 29–643, grey) and PSK-bound DcPSKR^{LRR} (residues 29–643, cyan) with a r.m.s.d. of 0.66 Å.

are homologous (Cα r.m.s.d. 1.49 Å over 600 amino acids) and an equivalent surface area is buried by their interaction with SERK1^{LRR} (984 Å^2) and SERK2^{LRR} (973 Å^2), respectively (Fig. 3b). SERK1^{LRR} binds the carboxy-terminal side of PSKR1^{LRR}, whereas PSKR1^{ID} contacts the amino-terminal side of SERK1^{LRR} (Fig. 3a). The structures of the two complexes are well aligned with that of the BRI1- but not the FLS2-containing complex (Extended Data Fig. 7b, c). Unlike the flg22- and brassinosteroid-mediated complexes[14,20,21], PSK is not directly involved in the PSKR1^{LRR}–SERK1^{LRR} or DcPSKR^{LRR}–SERK2^{LRR} interfaces (Fig. 3b). This is seemingly inconsistent with the PSK-promoted PSKR–SERK interaction. The structure of a free DcPSKR^{LRR} (Extended Data Table 1) revealed that its ID is completely disordered (Fig. 3c and Extended Data Fig. 7d), sharply contrasting with the well-defined ID in PSK-bound DcPSKR^{LRR} (Fig. 3d) or PSKR1^{LRR} (Fig. 1a). This demonstrates that PSK allosterically induces PSKR^{LRR}–SERK^{LRR} interaction.

PSKR1^{ID} interaction with the N-terminal side of SERK1^{LRR} is mainly mediated by van der Waals contacts (Fig. 4a). Centred at this interface is SERK1^{Thr59} that tightly packs against PSKR1^{Leu516} and PSKR1^{Tyr518}. Stacking of SERK1^{Phe61} against PSKR1^{Pro525} further fortifies the interactions around this interface (Fig. 4a, left panel). More extensive PSKR1^{LRR}–SERK1^{LRR} interactions come from contacts of the residues PSKR1^{Phe596}, PSKR1^{Ser598} and PSKR1^{Thr619} from one lateral side of PSKR1 with the inner surface of SERK1^{LRR} (Fig. 4a, right panel). The PSKR1^{LRR}–SERK1^{LRR} interactions are highly conserved in the PSK–DcPSKR^{LRR}–SERK2^{LRR} complex (Fig. 4b and Extended Data Fig. 1d).

DcPSKR(S608Y) and DcPSKR(T629Y), predicted to generate steric clashes with SERK2 (Fig. 4b, right panel), led to loss of PSK-induced DcPSKR^{LRR}–SERK2^{LRR} interaction (Fig. 4c, left panel and Extended Data Fig. 8a, b). A similar observation was also made for DcPSKR(F606D). Consistently, mutations of the equivalent residues PSKR1^{Phe596}, PSKR1^{Ser598} and PSKR1^{Thr619} (Fig. 4a) resulted in much less responsiveness to PSK for interaction with BAK1 in *Arabidopsis* protoplasts (Fig. 4c, right panel). Furthermore, mutations of these

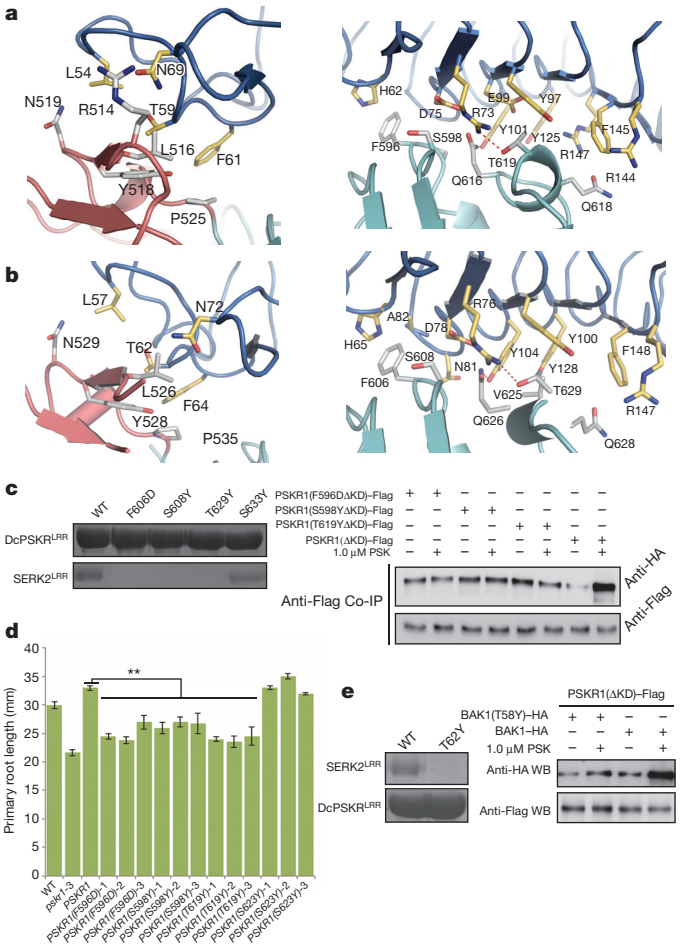

Figure 4 | Mutagenesis analysis of PSKR–SERK interaction. **a**, Detailed interactions of the ID (salmon, left) and the C-terminal side (cyan, right) of PSKR1^{LRR} with SERK1^{LRR} (blue). **b**, Detailed interactions of the ID (salmon, left) and the C-terminal side (cyan, right) of DcPSKR^{LRR} with SERK2^{LRR} (blue). **c**, Mutagenesis analysis of PSKR–SERK interaction. Left, interaction between WT or mutant DcPSKR^{LRR} and SERK2^{LRR} in the presence of PSK as assayed in Fig. 2a. Right, mutations of critical PSKR1 residues render PSKR1(ΔKD)–BAK1 interaction less sensitive to PSK in *Arabidopsis* protoplasts as assayed in Fig. 2c. Full blots are shown in Supplementary Data. **d**, Reducing PSKR–SERK interaction compromises *PSKR1* to complement the shortened root phenotypes of *pskr1-3* mutants. Average (±s.e.m.) primary root lengths of seedlings were determined in three independent experiments for each line ($n = 30$, $^{**}P < 0.01$, Student's *t*-test). **e**, Mutagenesis analysis of PSKR–SERK2^{T62}/BAK1^{T58} interaction. Left, SERK2(T62Y) disrupted PSK-induced DcPSKR^{LRR}–SERK2^{LRR} interaction in solution as assayed in Fig. 2a. Right, BAK1(T58Y) is less sensitive to PSK for interaction with PSKR1(ΔKD) as assayed in Fig. 2c. Full blots are shown in Supplementary Data.

PSKR1 residues but not the controls (PSKR1(S623Y) or DcPSKR(S633Y)) (Fig. 4c and Extended Data Fig. 8a, b) reduced the ability of *PSKR1* to complement the shorter roots of *pskr1-3* mutants and responsiveness of *Arabidopsis* plants to PSK (Fig. 4d and Extended Data Fig. 2c). SERK2(T62Y) is expected to generate similar effects on PSK-promoted PSKR–SERK interaction. Indeed, the SERK2^{LRR} mutant protein failed to form a PSK-induced complex with DcPSKR^{LRR} (Fig. 4e, left panel and Extended Data Fig. 8a, b). Consistently, mutation of the equivalent residue BAK1^{Thr58} (Extended Data Fig. 8c) rendered BAK1–PSKR1(ΔKD) interaction less responsive to PSK than wild-type BAK1 (Fig. 4e, right panel).

Our current study offers evidence that PSK promotes PSKR–SERK heterodimerization, providing a link between PSK perception and early intracellular signalling and further supporting the dimerization model[14]. Similar to brassinosteroid signalling[22], PSK signalling also

negatively regulates pathogen-associated molecular pattern (PAMP)-triggered immunity (PTI)[23,24]. However, expressions of disease-related genes were pathogen-induced in the *pskr1-3* mutant plants[23], similar to the *bri1* mutants[22], whereas the *bak1* or *bak1 bkk1* (*serk4*) mutants displayed constitutive immune responses even under sterile growing conditions[25,26]. Thus, the roles played by SERK members in plant growth and disease resistance seem to be uncoupled, similar to those of BAK1 in brassinosteroid and PTI signalling[27]. These results can be reconciled by a previous model[25,26] postulating that SERK members negatively regulate a brassinosteroid-independent cell-death pathway induced by pathogens, which can be antagonized by the PSK signalling. PSK-enhanced PSKR–SERK heterodimerization can lead to transphosphorylation of the two RKs. Indeed, kinase activity of PSKR1 is essential for PSK-induced plant growth in *Arabidopsis*[12].

Unlike flg22 and brassinosteroid, which mediate interactions between two LRR-RKs[14,20,21] by acting as 'molecular glue', PSK functions to stabilize the $PSKR^{ID}$, which in turn recruits a SERK member to form a stable PSKR–SERK complex, resulting in allosteric activation of PSKR. The $PSKR^{ID}$ is shorter than that of BRI1, which is well structured even in the absence of ligand[28,29]. It therefore seems that ligand binding is required to complete the $PSKR^{ID}$. Indeed, structural comparison showed that the $PSKR1^{ID}$ together with PSK is similarly positioned to $BRI1^{ID}$ (Extended Data Fig. 7b). It will be interesting to investigate whether RLPs and some other RKs that contain an ID with a similar size and position (relative to the last LRR) to that of PSKR[30] use this mechanism for interaction with their partners.

Online Content Methods, along with any additional Extended Data display items and Source Data, are available in the online version of the paper; references unique to these sections appear only in the online paper.

Received 30 March; accepted 24 June 2015.
Published online 26 August 2015.

1. Murphy, E., Smith, S. & De Smet, I. Small signaling peptides in *Arabidopsis* development: how cells communicate over a short distance. *Plant Cell* **24,** 3198–3217 (2012).
2. Matsubayashi, Y. Posttranslationally modified small-peptide signals in plants. *Annu. Rev. Plant Biol.* **65,** 385–413 (2014).
3. Matsubayashi, Y., Ogawa, M., Morita, A. & Sakagami, Y. An LRR receptor kinase involved in perception of a peptide plant hormone, phytosulfokine. *Science* **296,** 1470–1472 (2002).
4. Matsubayashi, Y., Ogawa, M., Kihara, H., Niwa, M. & Sakagami, Y. Disruption and overexpression of *Arabidopsis* phytosulfokine receptor gene affects cellular longevity and potential for growth. *Plant Physiol.* **142,** 45–53 (2006).
5. Matsubayashi, Y. & Sakagami, Y. Phytosulfokine, sulfated peptides that induce the proliferation of single mesophyll cells of *Asparagus officinalis* L. *Proc. Natl Acad. Sci. USA* **93,** 7623–7627 (1996).
6. Srivastava, R., Liu, J. X. & Howell, S. H. Proteolytic processing of a precursor protein for a growth-promoting peptide by a subtilisin serine protease in *Arabidopsis*. *Plant J.* **56,** 219–227 (2008).
7. Komori, R., Amano, Y., Ogawa-Ohnishi, M. & Matsubayashi, Y. Identification of tyrosylprotein sulfotransferase in *Arabidopsis*. *Proc. Natl Acad. Sci. USA* **106,** 15067–15072 (2009).
8. Kutschmar, A. *et al.* PSK-alpha promotes root growth in *Arabidopsis*. *New Phytol.* **181,** 820–831 (2009).
9. Stührwohldt, N., Dahlke, R. I., Steffens, B., Johnson, A. & Sauter, M. Phytosulfokine-alpha controls hypocotyl length and cell expansion in *Arabidopsis* thaliana through phytosulfokine receptor 1. *PLoS ONE* **6,** e21054 (2011).
10. Amano, Y., Tsubouchi, H., Shinohara, H., Ogawa, M. & Matsubayashi, Y. Tyrosine-sulfated glycopeptide involved in cellular proliferation and expansion in *Arabidopsis*. *Proc. Natl Acad. Sci. USA* **104,** 18333–18338 (2007).
11. Morillo, S. A. & Tax, F. E. Functional analysis of receptor-like kinases in monocots and dicots. *Curr. Opin. Plant Biol.* **9,** 460–469 (2006).
12. Hartmann, J., Fischer, C., Dietrich, P. & Sauter, M. Kinase activity and calmodulin binding are essential for growth signaling by the phytosulfokine receptor PSKR1. *Plant J.* **78,** 192–202 (2014).
13. Belkhadir, Y., Yang, L., Hetzel, J., Dangl, J. L. & Chory, J. The growth-defense pivot: crisis management in plants mediated by LRR-RK surface receptors. *Trends Biochem. Sci.* **39,** 447–456 (2014).
14. Han, Z., Sun, Y. & Chai, J. Structural insight into the activation of plant receptor kinases. *Curr. Opin. Plant Biol.* **20,** 55–63 (2014).
15. Chinchilla, D., Shan, L., He, P., de Vries, S. & Kemmerling, B. One for all: the receptor-associated kinase BAK1. *Trends Plant Sci.* **14,** 535–541 (2009).
16. Hanai, H. *et al.* A secreted peptide growth factor, phytosulfokine, acting as a stimulatory factor of carrot somatic embryo formation. *Plant Cell Physiol.* **41,** 27–32 (2000).
17. Schmidt, E. D., Guzzo, F., Toonen, M. A. & de Vries, S. C. A leucine-rich repeat containing receptor-like kinase marks somatic plant cells competent to form embryos. *Development* **124,** 2049–2062 (1997).
18. Wang, X. *et al.* Sequential transphosphorylation of the BRI1/BAK1 receptor kinase complex impacts early events in brassinosteroid signaling. *Dev. Cell* **15,** 220–235 (2008).
19. Heyman, J. *et al.* ERF115 controls root quiescent center cell division and stem cell replenishment. *Science* **342,** 860–863 (2013).
20. Sun, Y. *et al.* Structural basis for flg22-induced activation of the *Arabidopsis* FLS2–BAK1 immune complex. *Science* **342,** 624–628 (2013).
21. Santiago, J., Henzler, C. & Hothorn, M. Molecular mechanism for plant steroid receptor activation by somatic embryogenesis co-receptor kinases. *Science* **341,** 889–892 (2013).
22. Albrecht, C. *et al.* Brassinosteroids inhibit pathogen-associated molecular pattern-triggered immune signaling independent of the receptor kinase BAK1. *Proc. Natl Acad. Sci. USA* **109,** 303–308 (2012).
23. Igarashi, D., Tsuda, K. & Katagiri, F. The peptide growth factor, phytosulfokine, attenuates pattern-triggered immunity. *Plant J.* **71,** 194–204 (2012).
24. Mosher, S. *et al.* The tyrosine-sulfated peptide receptors PSKR1 and PSY1R modify the immunity of *Arabidopsis* to biotrophic and necrotrophic pathogens in an antagonistic manner. *Plant J.* **73,** 469–482 (2013).
25. He, K. *et al.* BAK1 and BKK1 regulate brassinosteroid-dependent growth and brassinosteroid-independent cell-death pathways. *Curr. Biology* **17,** 1109–1115 (2007).
26. Kemmerling, B. *et al.* The BRI1-associated kinase 1, BAK1, has a brassinolide-independent role in plant cell-death control. *Curr. Biology* **17,** 1116–1122 (2007).
27. Schwessinger, B. *et al.* Phosphorylation-dependent differential regulation of plant growth, cell death, and innate immunity by the regulatory receptor-like kinase BAK1. *PLoS Genet.* **7,** e1002046, CrossRef (2011).
28. She, J. *et al.* Structural insight into brassinosteroid perception by BRI1. *Nature* **474,** 472–476 (2011).
29. Hothorn, M. *et al.* Structural basis of steroid hormone perception by the receptor kinase BRI1. *Nature* **474,** 467–471 (2011).
30. Fritz-Laylin, L. K., Krishnamurthy, N., Tor, M., Sjolander, K. V. & Jones, J. D. Phylogenomic analysis of the receptor-like proteins of rice and *Arabidopsis*. *Plant Physiol.* **138,** 611–623 (2005).

Supplementary Information is available in the online version of the paper.

Acknowledgements We thank S. Huang and J. He for assistance with data collection, J. Li for the *serk1*, *serk2*, *bak1* single and triple mutant seeds and W. Li and W. Chu for providing facility support. This research was funded by Projects of International Cooperation and Exchanges NSFC (31420103906), Chinese Ministry of Science and Technology (2015CB910200) and State Key Program of National Natural Science of China (31130063) to J.C.; Chinese Natural Science Foundation (31330053) to W.Y. and Ministry of Science and Technology of China (2015CB910202) to H.L.

Author Contributions J.C., W.Y., J.W., H.L. and Z.H. designed the experiments. J.W., H.L., H.Z., T.W. and G.L. performed the experiments. Data were analysed by J.C., W.Y., J.W., H.L. and J.C.; J.C., W.Y., J.W., H.L. and Z.H. contributed to manuscript preparation. J.C. wrote the manuscript.

Author Information The atomic coordinates and structure factors have been deposited in the Protein Data Bank. The PDB code of free $DcPSKR^{LRR}$ is 4Z62. The PDB codes of PSK–$PSKR1^{LRR}$ and PSK–$DcPSKR^{LRR}$ are 4Z63 and 4Z5W, respectively. The PDB codes of PSK–$PSKR1^{LRR}$–$SERK1^{LRR}$ and PSK–$DcPSKR^{LRR}$–$SERK2^{LRR}$ are 4Z64 and 4Z61, respectively. Reprints and permissions information is available at www.nature.com/reprints. The authors declare no competing financial interests. Readers are welcome to comment on the online version of the paper. Correspondence and requests for materials should be addressed to J.C. (chaijj@mail.tsinghua.edu.cn) or W.Y. (wcyang@genetics.ac.cn).

METHODS

No statistical methods were used to predetermine sample size and the experiments were not randomized.

Protein expression and purification. The constructs of DcPSKR^{LRR} (residues 24–659), PSKR1^{LRR} (residues 24–648), SERK1^{LRR} (residues 1–213, N115D, N163Q), SERK2^{LRR} (residues 1–216) and BAK1^{LRR} (residues 1–220) with a C-terminal 6 × His tag were generated by standard PCR-based cloning strategy and their identities were confirmed by sequencing. DcPSKR^{LRR} and PSKR1^{LRR} constructs were expressed in High Five insect cells at 22 °C using the pFastBac-1 vector (Invitrogen) with a modified N-terminal hemolin signal peptide, and SERK1^{LRR}, SERK2^{LRR} and BAK1^{LRR} constructs used the original pFastBac-1 vector. One litre of cells (2.0×10^6 cells ml^{-1} cultured in the medium from Expression Systems) was infected with 20 ml recombinant baculovirus and the media was harvested after 48 h. The proteins were purified using Ni-NTA (Novagen) and size-exclusion chromatography (Hiload200, GE Healthcare) in buffer containing 10 mM Bis-Tris pH 6.0 and 100 mM NaCl. The purified proteins were digested with endoglycosidase F1 and F3 at 18 °C overnight and further cleaned using gel filtration. The deglycosylated DcPSKR^{LRR} and PSKR1^{LRR} proteins were concentrated to about 7.0 mg ml^{-1} for crystallization. To crystallize the PSK–DcPSKR^{LRR}–SERK2^{LRR} complex, the purified DcPSKR^{LRR}, SERK2^{LRR} and the PSK peptide (synthesized by Scilight Biotechnology, China) were mixed and incubated at 4 °C for 20 min. The mixture was subsequently subjected to gel filtration (Hiload200, GE Healthcare) in buffer containing 10 mM Bis-Tris pH 6.0, 100 mM NaCl. The purified complex was concentrated to about 7.0 mg ml^{-1} for crystallization. Similar procedures were used for purification of the PSK–PSKR1^{LRR}–SERK1^{LRR} complex.

Crystallization, data collection, structure determination and refinement. Crystallization experiments were performed with hanging-drop vapour-diffusion methods by mixing equal volumes (1.0 μl) of protein and reservoir solution at 18 °C. Good quality crystals of DcPSKR^{LRR} were obtained in buffer containing 0.1 M Tris pH 8.5, 2.0 M $(NH_4)_2SO_4$. For crystallization of PSK–DcPSKR^{LRR} or PSK–PSKR1^{LRR} complex, a mixture of DcPSKR^{LRR} or PSKR1^{LRR} and PSK peptide with a molar ratio of 1:5 was used for crystallization. Diffraction quality crystals of PSK–DcPSKR^{LRR} were obtained in buffer containing 0.3 M KH_2PO_4, 20% PEG(2,000) within 3 days, and for PSK–PSKR1^{LRR}, good quality crystals appeared in buffer containing 0.1 M Bis-Tris pH 5.5, 2.0 M $(NH_4)_2SO_4$ within 6 months. Diffraction quality crystals of the PSK–DcPSKR^{LRR}–SERK2^{LRR} complex were obtained in buffer containing 0.1 M sodium citrate pH 5.5, 0.4 M KCl, 30% v/v pentaerythritol propoxylate (5/4 PO/OH) within one week, and for PSK–PSKR1^{LRR}–SERK1^{LRR}, high quality crystals emerged in buffer containing 0.1 M sodium acetate pH 4.5, 2.0 M $(NH_4)_2SO_4$ over 6 months. All the diffraction data were collected at the Shanghai Synchrotron Radiation Facility (SSRF) on beam line BL17U1 using a CCD detector. The data were processed using HKL2000 (ref. 31). The crystal structure of PSK–DcPSKR^{LRR} was determined by molecular replacement (MR) with PHASER[32] using the structure of FLS2 (PDB code: 4MN8) as the initial searching model. The model from MR was built with the program COOT[33] and subsequently subjected to refinement by the program Phenix[34]. The other crystal structures were determined by MR using the structure of DcPSKR^{LRR} as the initial searching model. All the five crystal structures were refined by the program Phenix[34] with excellent stereochemistry (Extended Data Table 1). All the figures representing structures were prepared using PYMOL[35].

Microscale thermophoresis assay. The microscale thermophoresis (MST) assay was performed as previously described[36]. The affinity of the purified DcPSKR^{LRR} (or its mutants) with PSK (or dPSK) was measured using the Monolith NT.115 from Nanotemper Technologies. Proteins were fluorescently labelled according to the manufacturer's protocol and the labelled protein used for each assay was about 200 nM. A solution of unlabelled peptide was diluted for appropriate serial concentration gradient. The samples were loaded into silica capillaries (Polymicro Technologies) after incubation at room temperature for 30 min. Measurements were performed at 20 °C in buffer containing 20 mM citric acid pH 5.0, 50 mM NaCl, and 0.05% Tween 20, by using 12% LED power and 40% MST power. The assays were repeated three times for each affinity measurement. Data analyses were performed using Nanotemper Analysis software and OriginPro 8.0 software provided by the manufacturer.

Gel filtration assay. The PSKR1^{LRR} and SERK1^{LRR} proteins purified as described above were subjected to gel filtration analysis (Hiload200, GE Healthcare) in the presence or absence of PSK. The PSKR1^{LRR}, SERK1^{LRR} proteins and PSK with a molar ratio of about 1:2:3 was mixed and incubated in 4 °C for 20 min before the gel filtration analysis in buffer containing 10 mM Bis-Tris pH 6.0, 100 mM NaCl. Samples from relevant fractions were applied to SDS–PAGE and visualized by Coomassie blue staining. Similar procedures were used for other interaction analysis of PSKR^{LRR}–SERK^{LRR}. The DcPSKR^{LRR} and SERK2^{LRR} mutants designed to disrupt their interaction were also verified with the gel filtration assay described above.

Sedimentation-velocity analytical ultracentrifugation. Sedimentation velocity was performed with an XL-I analytical ultracentrifuge (Beckman Coulter) equipped with a four-cell An-60 Ti rotor for interaction analysis of PSKR1^{LRR} and SERK2^{LRR} in the presence or absence of PSK at 20 °C. For PSKR1^{LRR} and SERK1^{LRR} or BAK1^{LRR}, an eight-cell An-50 Ti rotor was used. The molar ratio of PSKR1^{LRR}, SERKs^{LRR} proteins and PSK is about 1:2:3, and the total OD_{280} is about 1.0. Buffer containing 10 mM Bis-Tris pH 6.0, 100 mM NaCl was used as the reference solution. All samples were applied at a speed of 45,000 rpm. Absorbance scans were taken at 280 nm at the intervals of 0.003 cm size in a radical direction. The different sedimentation coefficients, $c(s)$, and molecular weight were calculated by SEDFIT V14.4f software.

Plant materials and growth conditions. *Arabidopsis thaliana* wild type Col-0 and *pskr1-3* (SALK_008585) were obtained from *Arabidopsis* Biological Resource Center and reported to be a null mutant[8]. *serk1-8*, *serk2-1*, *bak1-4* and *serk1-8*−/+ *serk2-1*−/−*bak1-4*−/− triple mutant were generously provided by J. Li and each single mutant has been identified to be null[37]. Seeds were surface sterilized for 5 min in 20% $NaClO_3$ followed by 5 times of wash using sterile H_2O and dispersed on 1/2 Murashige & Skoog (MS) media containing 1% agar and 10 g l^{-1} sucrose, pH 5.8, in Petri dish. For PSK treatment of the seedlings, PSK was added in the MS media to different final concentrations. The sterilized seeds were vernalized for 3 days at 4 °C and grown for 10 days in normal condition (16 h of light/8 h of dark, 22–23 °C).

Generation of constructs and plant transformation. For stable transgenic plants, we generated the constructs of *PSKR1* coding sequences with different site mutations by subcloning the sequences into the pDONOR207 (Invitrogen) vector to the destination vector pWA43 or pWA53 by gateway recombination strategy (for PSKR1, DcPSKR, F506A, R300A, W448A, T398L and D445A, the final target vector is pWA43; for F596D, S598Y, T619Y, S623Y and DcPSKR^{ECD}–PSKR1^{KD}, the target vector is pWA53). pWA43 (hygromycin resistant in plants) and pWA53 (kanamycin resistant in plant) contained a CaMV 35S promoter driven C-terminal GFP coding sequence with the recombination sites in between and terminated by a 35S terminator. For the constructs used for transient protoplast transformation, the truncated PSKR1 coding sequence (PSKR1(ΔKD)) with the kinase domain deleted was fused with a C-terminal 3× Flag affinity tag and inserted into the backbone of pBSK-35S: 35STerminator after digestion with SmaI. For SERK1, SERK2, BAK1 and BAK1(T58Y) transient expression, the full-length coding sequences were inserted to pUC-SPYCE[38] which contains a C-terminal haemagglutinin affinity tag after digestion with SmaI. For co-expression *in planta*, SERK1, SERK2 and BAK1 inserted to PSPYCE-35S (kanamycin resistant in plant), which contains the same framework with pUC-SPYCE, were transformed to the T1 generation of pWA43-PSKR1 plants in the *pskr1-3* background. The transgenic plants were isolated by double selection on MS media containing kanamycin and hygromycin. *Arabidopsis* was transformed with these constructs by *Agrobacterium tumefaciens* (GV3101) by the floral dip method[39].

Root length measurement and statistical analysis. For each construct, ten transgenic overexpression lines in the *pskr1-3* mutant background were analysed and three lines representative for all lines were selected to present. 10-days seedlings grown in the greenhouse from the lines with *PSKR1* transcripts detected were subjected to primary root length measurement from photographs using Image J (National Institutes of Health, http://rsb.info.nih.gov/ij). To keep consistent seed fitness, only newly collected seeds at the same time were used for the assay. For each genotype, three independent experiments were performed. Student's *t*-test was performed to test statistical significance of means.

PSK treatment and co-immunoprecipitation assay. Protoplast transformation was performed according to the reported method[40] and cultured for 12 h at 22 °C. For each transformation, the culture of the transformed protoplasts was divided equally into two 50 ml centrifuge tubes. PSK peptide (diluted in H_2O) was added to the final concentration of 1.0 μM in one tube and the same volume of H_2O was added as mock treatment in the other tube. After 15 min of the treatment, the cells were harvested and lysed for 2 min in the lysis buffer (50 mM HEPES-KOH pH 7.5, 0.15 M KCl, 0.001 M EDTA, 0.1% Triton-X 100, 0.001 M DTT with freshly added proteinase inhibitor cocktail, (Roche)). The lysate was centrifuged at 10,000*g* for 10 min and the supernatant was subjected to coimmunoprecipitation (Co-IP) with agarose-conjugated anti-Flag antibody (Sigma-Aldrich, Cat. A220) for 3 h at 4 °C. The agarose beads were washed with the lysis buffer for 6 times, diluted in 1× sample loading buffer and boiled for 5 min before SDS–PAGE. The following immunoblot was performed according to the standard procedure with anti-Flag (Sigma-Aldrich, Cat. F1804) and anti-HA antibody (Santa Cruz, Cat. sc-7392). For the Co-IP *in planta*, equal amounts of 14 days seedlings from the same transgenic lines (overexpressing PSKR1–GFP and SERK1/2/3–HA or PSKR1–GFP alone as a negative control) were treated on the MS media supplemented

with 1.0 μM PSK and the MS media without PSK for 12 h. Then 5 g of the treated and untreated seedlings were collected and lysed for the following Co-IP experiments. GFP-trap agarose beads (ChromoTek, Cat. gta-200) were used for the affinity binding of the PSKR1–GFP fusion protein and anti-GFP-HRP (Miltenyi Biotec, Cat. 130-091-833) was used to detect the GFP epitope and anti-HA antibody for HA epitope. Each Co-IP experiment was repeated at least three times.

31. Otwinowski, Z. & Minor, W. Processing of X-ray diffraction data collected in oscillation mode. *Methods Enzymol.* **276,** 307–326 (1997).
32. McCoy, A. J. *et al.* Phaser crystallographic software. *J. Appl. Crystallogr.* **40,** 658–674 (2007).
33. Emsley, P. & Cowtan, K. Coot: model-building tools for molecular graphics. *Acta Crystallogr. D* **60,** 2126–2132 (2004).
34. Adams, P. D. *et al.* PHENIX: building new software for automated crystallographic structure determination. *Acta Crystallogr. D* **58,** 1948–1954 (2002).
35. DeLano, W. L. PyMOL Molecular Viewer (http://www.pymol.org) (2002).
36. Jerabek-Willemsen, M., Wienken, C. J., Braun, D., Baaske, P. & Duhr, S. Molecular interaction studies using microscale thermophoresis. *Assay Drug Dev. Technol.* **9,** 342–353 (2011).
37. Gou, X. *et al.* Genetic evidence for an indispensable role of somatic embryogenesis receptor kinases in brassinosteroid signaling. *PLoS Genet.* **8,** e1002452 (2012).
38. Walter, M. *et al.* Visualization of protein interactions in living plant cells using bimolecular fluorescence complementation. *Plant J.* **40,** 428–438 (2004).
39. Clough, S. J. & Bent, A. F. Floral dip: a simplified method for *Agrobacterium*-mediated transformation of *Arabidopsis thaliana. Plant J.* **16,** 735–743 (1998).
40. Yoo, S.-D., Cho, Y.-H. & Sheen, J. *Arabidopsis* mesophyll protoplasts: a versatile cell system for transient gene expression analysis. *Nature Protocols* **2,** 1565–1572 (2007).

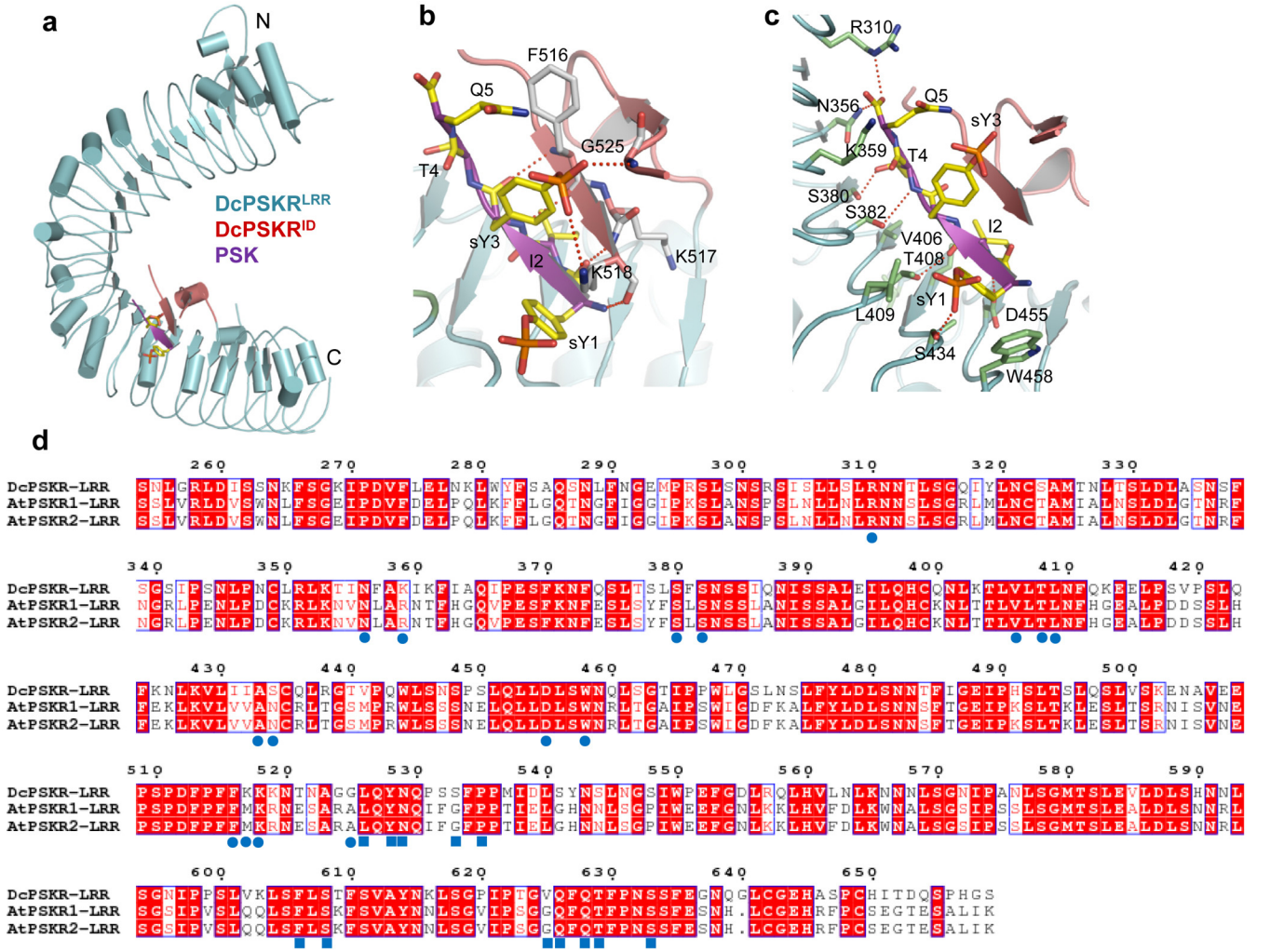

Extended Data Figure 1 | Recognition mechanism of PSK by PSKRs^{LRR} is highly conserved. **a**, Overall structure of PSK–DcPSKR^{LRR} complex. The sulfated tyrosines of PSK are shown in stick. Colour codes are indicated. ID, island domain; N, N terminus; C, C terminus. **b**, Detailed interactions between PSK (purple) and the island domain (salmon) of DcPSKR^{LRR}. Dashed lines indicate polar interactions. **c**, Detailed interactions between PSK and the inner side (cyan) of DcPSKR^{LRR}. **d**, PSKRs are conserved in PSK perception and interaction with SERKs. Sequence alignment of the ectodomains of carrot DcPSKR and *Arabidopsis* PSKR1/2. Conserved and similar residues are boxed with red ground and red font, respectively. Residues involved in recognition of PSK and interaction with a SERK member are indicated with blue solid circles and squares at the bottom, respectively.

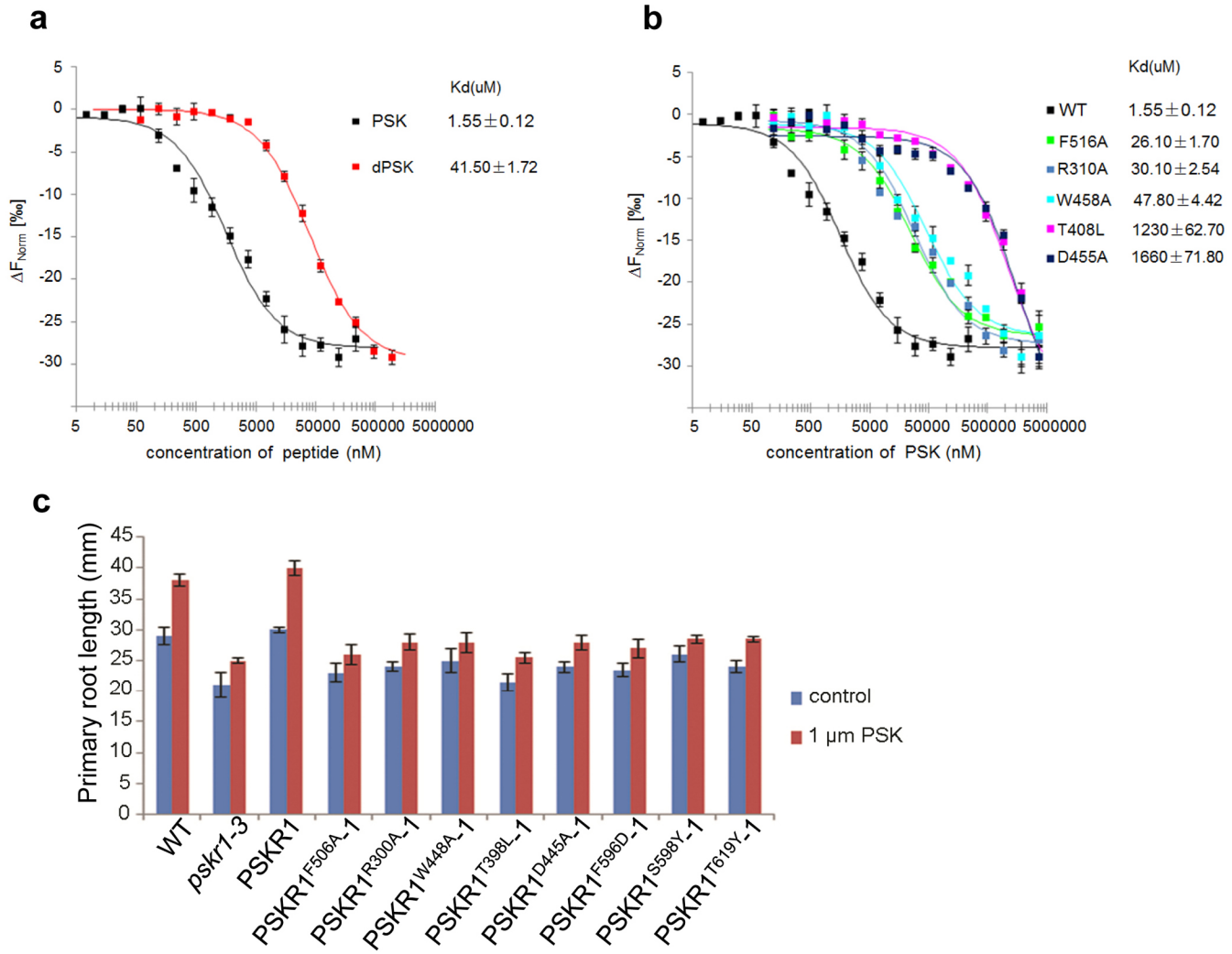

Extended Data Figure 2 | Mutagenesis analysis of PSKR recognition of PSK and PSKR–SERK interaction. **a**, Sulfation enhances PSK interaction with DcPSKR^{LRR}. Quantification of binding affinity between DcPSKR^{LRR} and PSK or the desulfated peptide (dPSK) by MST (MicroScale Thermophoresis). Data points indicate the difference in normalized fluorescence (‰) generated by PSK or dPSK binding DcPSKR^{LRR} protein, and curves indicate the calculated fits. Error bars represent standard error of 3 independent measurements. **b**, Mutagenesis analysis of DcPSKR^{LRR} by MST. Quantification of binding affinity between WT DcPSKR^{LRR} or various mutants as indicated and PSK by MST. Error bars represent standard error of 3 independent measurements. **c**, *pskr1-3* plants transformed with mutated *PSKR1* which compromised PSK or SERKs binding are less responsive to PSK than wild type or *pskr1-3* transformed with *PSKR1*. The line was the same as that used in Fig. 1e and 4d. Average (±s.e.m.) primary root lengths of seedlings were determined in three independent experiments with 30 seedlings analysed per genotype in the presence or absence of 1.0 μM PSK.

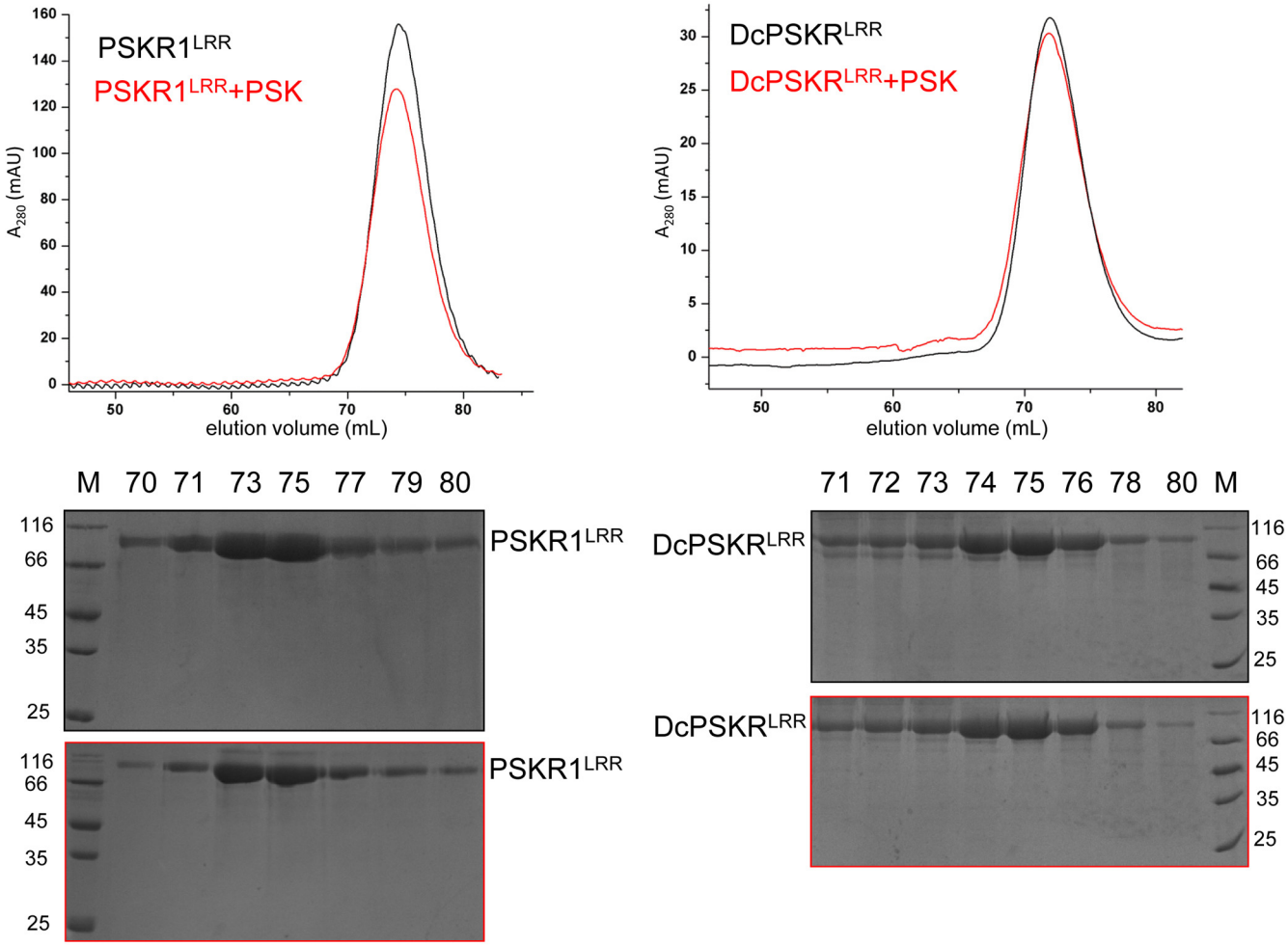

Extended Data Figure 3 | PSK binding induces no oligomerization of PSKR^{LRR}. Shown on the top is superposition of the gel filtration chromatograms of the PSKR1^{LRR} (left) or DcPSKR^{LRR} (right) protein in the absence (grey) and presence (red) of PSK. The vertical and horizontal axes represent ultraviolet absorbance (λ = 280 nm) and elution volume (ml), respectively. Bottom, Coomassie blue staining of the peak fractions shown on the top following SDS–PAGE. M, molecular weight ladder (kDa).

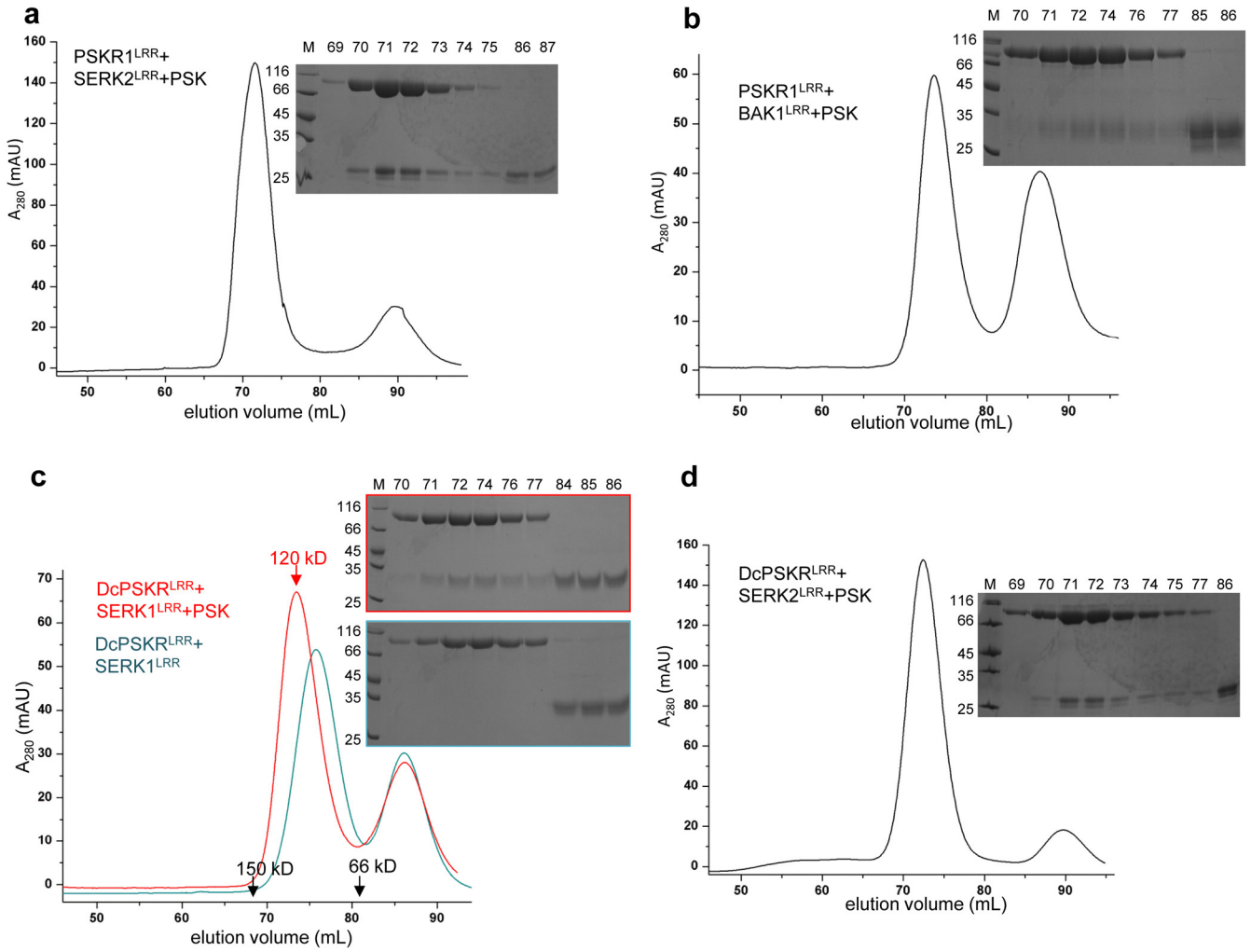

Extended Data Figure 4 | PSK induces PSKR1^{LRR} or DcPSKR^{LRR} interaction with SERK members in gel filtration. **a**, PSK induces PSKR1^{LRR}–SERK2^{LRR} heterodimerization. Right, Coomassie blue staining of the peak fractions shown on the left following SDS–PAGE. M, molecular weight ladder (kDa). **b**, PSK induces PSKR1^{LRR} heterodimerization with BAK1^{LRR}. The assay was performed as described in **a**. **c**, PSK induces DcPSKR^{LRR} heterodimerization with SERK1^{LRR}. The assays were performed as described in **a**. The red and black arrows indicate the elution position of PSK–DcPSKR^{LRR}–SERK1^{LRR} and the retention volumes of molecular weight markers, respectively. **d**, PSK induces DcPSKR^{LRR} heterodimerization with SERK2^{LRR}. The assay was performed as described in **a**.

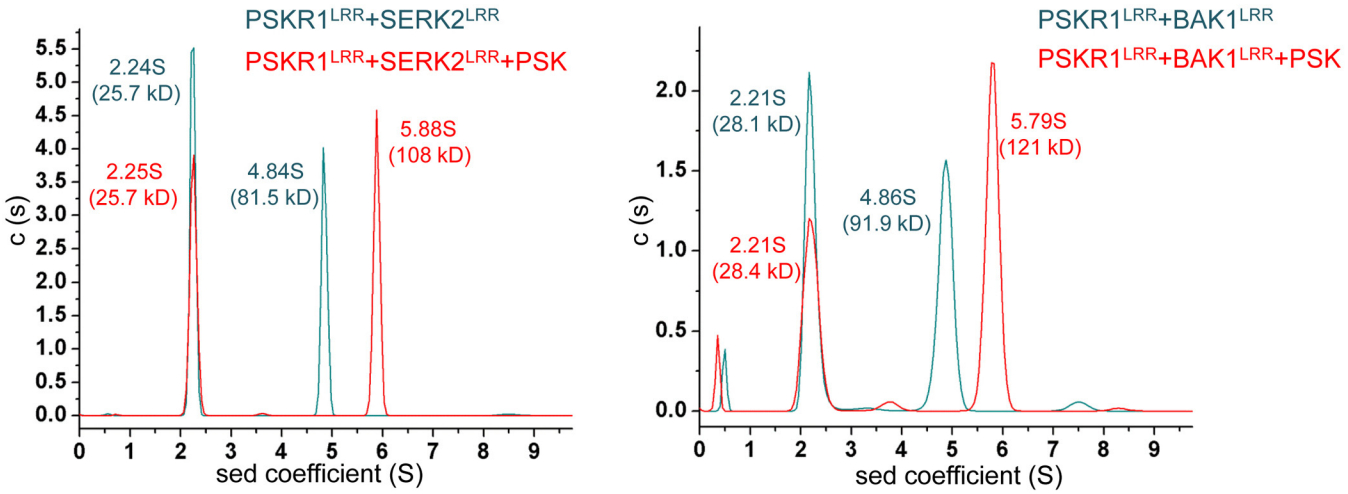

Extended Data Figure 5 | PSK induces PSKR1^{LRR} interaction with SERK members in sedimentation-velocity analytical ultracentrifugation. PSK induces PSKR1^{LRR}–SERK2^{LRR} (left panel) or PSKR1^{LRR}–BAK1^{LRR} (right panel) interaction in sedimentation-velocity analytical ultracentrifugation assays. The assays were performed as described in Fig. 2b. The glycoprotein nature of PSKR1^{LRR} may confer to the slight difference of calculated molecular weights. PSK induced the formation of a monomeric PSK–PSKR1^{LRR}–SERK2^{LRR} or PSK–PSKR1^{LRR}–BAK1^{LRR} complex, leading to the shift of PSKR1^{LRR} to a higher S.

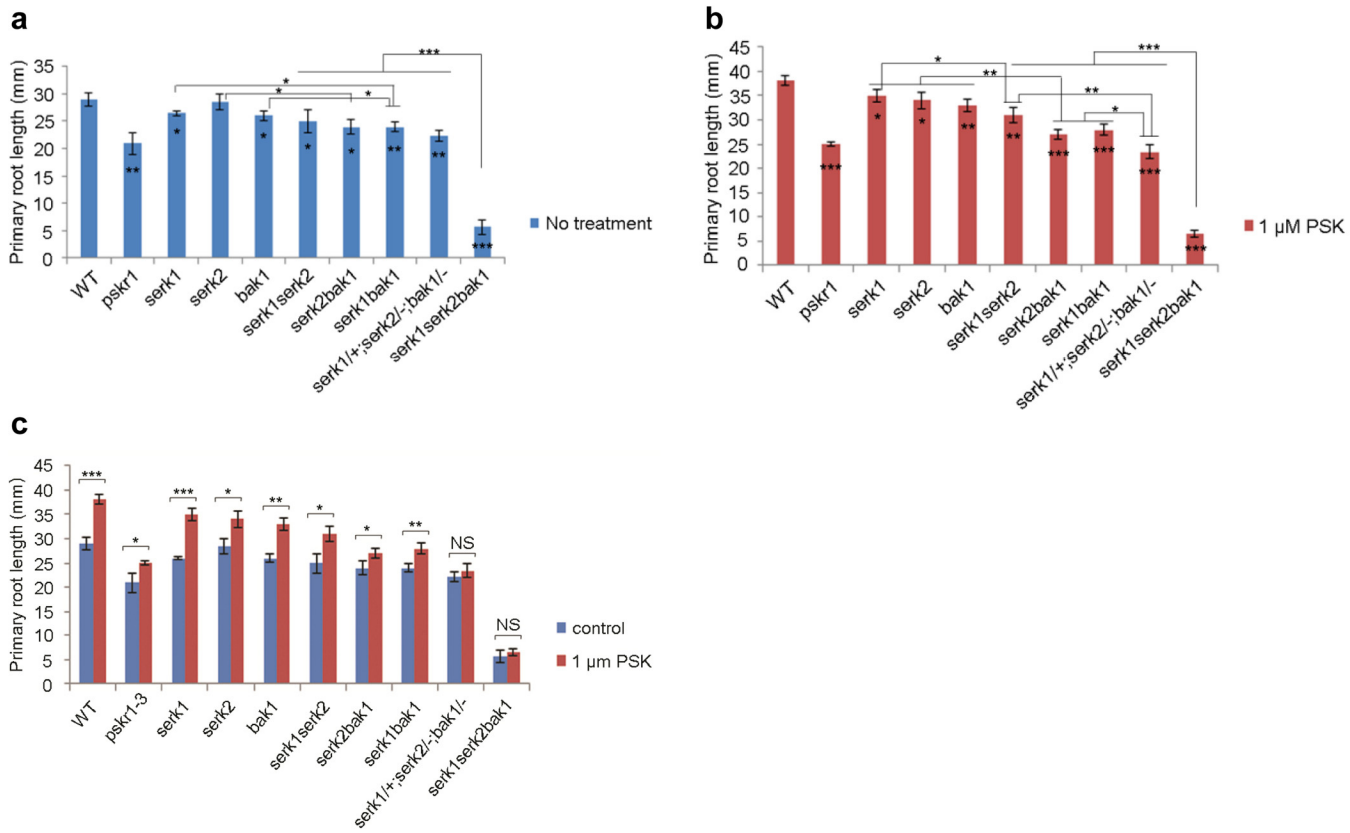

Extended Data Figure 6 | SERK members function redundantly in PSK-induced plant growth. **a**–**c**, Average (±s.e.m.) primary root lengths of seedlings were determined for the wild-type or *SERK* knockout *Arabidopsis* plants grown for 10 days on plates with (red) or without (blue) 1.0 μM PSK. Three independent experiments per genotype with 30 seedlings were performed. The statistics are shown in **a**, **b** and **c**. All the genotypes are compared in the absence of PSK in **a** and in the presence of PSK in **b**. The single or double *SERK* knockout plants only showed slightly shortened roots compared to the triple mutants. Asterisks within the bars indicate significant difference between the wild type and *SERK* knockout mutants and those above the bars indicate significant difference between different *SERK* knockout mutants. Each genotype in the presence and absence of PSK is compared in **c**. Student's *t*-test, $*P < 0.05$, $**P < 0.01$, $***P < 0.001$. NS, non-significant ($P > 0.05$).

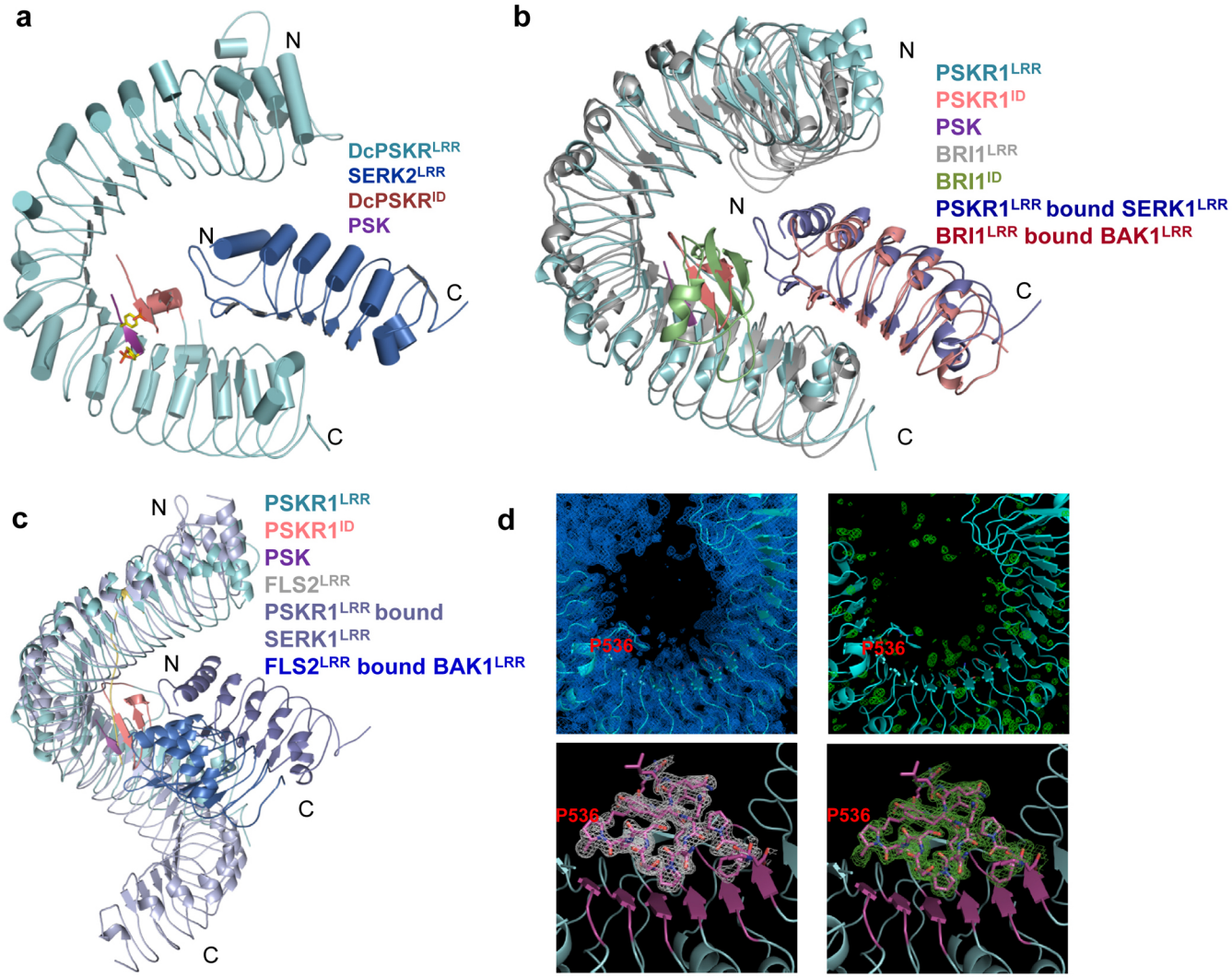

Extended Data Figure 7 | Different mechanism of PSK induced PSKR–SERK interaction compared to BRI1– BAK1 or FLS2–BAK1 complex. **a**, Overall structure of PSK–DcPSKR^{LRR}–SERK2^{LRR} complex. **b**, Structural comparison of PSK–PSKR1^{LRR}–SERK1^{LRR} and brassinosteroid–BRI1^{LRR}–BAK1^{LRR}. The structure of PSKR1^{LRR} (residues 77–634) was used as the template for alignment with that of BRI1 (residues 174–766; PDB code 4M7E) with a r.m.s.d. of 2.43 Å. **c**, Structural comparison of PSK–PSKR1^{LRR}–SERK1^{LRR} and flg22–FLS2^{LRR}–BAK1^{LRR}. The structure of PSKR1^{LRR} (residues 82–554) was used as the template for alignment with that of FLS2 (residues 79–509; PDB code 4MN8) with a r.m.s.d. of 4.4 Å. SERK1^{LRR} bound by PSKR1^{LRR} rotates about 30 degrees and shifts about 20 Å relative to the BAK1^{LRR}-bound FLS2^{LRR}. **d**, Electron density around the island domain of DcPSKR^{LRR} and PSK-bound DcPSKR^{LRR} in the finally refined structures. Top panel, electron density $2F_o - F_c$ (left) and $F_o - F_c$ (right) contoured at 1.30 sigma and 2.7 sigma, respectively, for the finally refined free DcPSKR^{LRR} structure. Bottom panel: electron density $2F_o - F_c$ (left) and $F_o - F_c$ (right) omitted around the island domain in the structure of PSK-bound DcPSKR^{LRR}. The island domain (residues 511–535) and the β–sheet (residues 474–480, 450–456, 427–432, 402–408, 376–381 and 352–357) interacting with the ID were not included in refinement and electron density calculation. All the deleted residues are shown in pink. The marker residue proline 536 is shown in red.

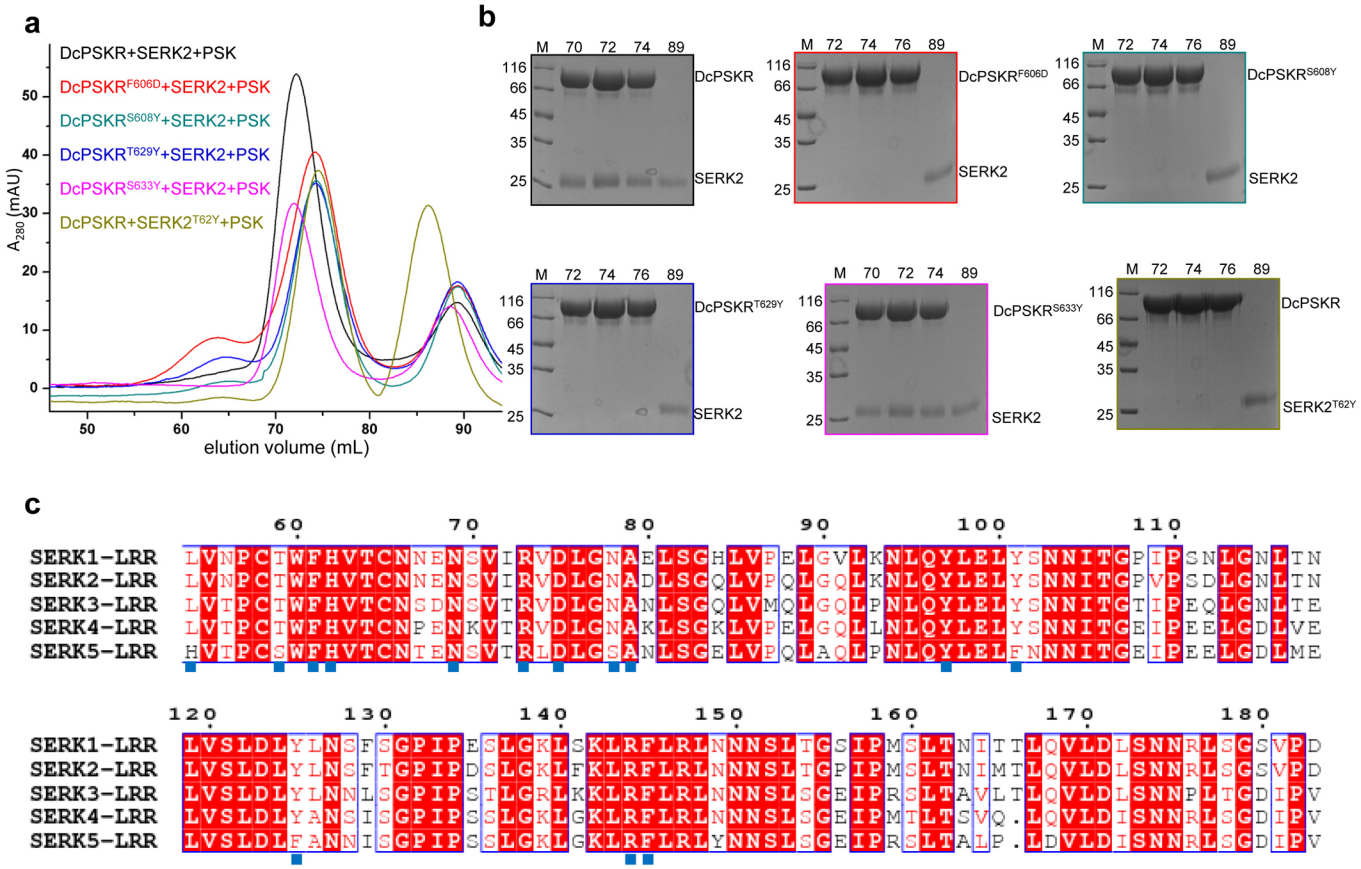

Extended Data Figure 8 | Mutagenesis analysis of DcPSKR^{LRR}–SERK2^{LRR} interaction. **a**, Superposition of the gel filtration chromatograms of the mutant DcPSKR^{LRR} and SERK2^{LRR} proteins in the presence of PSK. The assays were performed as described in Extended Data Fig. 4a. **b**, Coomassie blue staining of the peak fractions shown on the left chromatograms following SDS–PAGE. M, molecular weight ladder (kDa). **c**, The amino acids of SERKs involved in PSKRs interaction are conserved. Sequence alignment of the ectodomains of SERK family proteins. Conserved and similar residues are boxed with red ground and red font, respectively. Residues involved in interaction with PSKR are indicated with blue solid squares at the bottom. The sequence of SERK3 is 100% identical to BAK1.

Extended Data Table 1 | Data collection and refinement statistics

Data set	DcPSKR^{LRR}	PSK-DcPSKR^{LRR}	PSK-DcPSKR^{LRR}-SERK2^{LRR}	PSK-PSKR1^{LRR}	PSK-PSKR1^{LRR}-SERK1^{LRR}
Wavelength (Å)	1.000	1.000	1.000	1.000	1.000
Resolution (Å)	99.0-2.9	99.0-2.2	99.0-2.75	99.0-2.5	99.0-2.65
	(2.95-2.9)	(2.24-2.2)	(2.8-2.75)	(2.54-2.5)	(2.7-2.65)
Space group	$C222_1$	P1	C2	$P4_322$	$C222_1$
a, b, c (Å)	90.0,98.8, 227.3	66.7, 75.7, 93.9	486.2, 73.5, 67.3	92.9,92.9, 242.5	152.5, 220.9, 105.4
α, β, γ (°)	90.0, 90.0, 90.0	111.3, 105.7, 97.2	90.0, 95.8, 90.0	90.0, 90.0, 90.0	90.0, 90.0, 90.0
Unique reflections	21,448(1,019)	78,850(2,566)	54,320(2,762)	36,529(1,779)	49,329(2,490)
Completeness	93.6% (92.6%)	97.3% (87.0%)	88.8% (87.0%)	98.4% (99.6%)	96.8% (98.8%)
Rsym (%)	12.6(47.4)	7.4(54.9)	7.9(40.9)	10.3(56.6)	10.0 (48.4)
redundancy	5.3(5.3)	3.9(3.9)	2.0(1.9)	5.3(5.7)	4.2(4.2)
I/δ	18.5(6.4)	17.9(5.9)	14.7(3.1)	26.0(4.4)	15.5(2.65)
Statistics for refinement					
Resolution (Å)	99-2.9	99.0-2.2	99.0-2.75	99.0-2.5	99.0-2.66
	(3.03-2.9)	(2.23-2.20)	(2.8-2.75)	(2.58-2.5)	(2.71-2.66)
No. of RFs	21,401(2,391)	78,850(2,566)	54,303(2,613)	36,369(2,715)	49,253(2,282)
Completeness	93.4%	97.1%	87.7%	98.1%	95.7%
Rwork/Rfree	20.2 (24.9)/	21.2(29.0)/	20.0(24.2)/	22.9(26.7)/	20.0(28.6) /
(%)	25.4(32.6)	26.2(33.7)	26.2(38.3)	27.6(35.1)	24.6(36.7)
R.m.s.d					
Bond (degree)	1.418	1.389	1.445	1.481	1.265
length (Å)	0.008	0.008	0.008	0.008	0.008
Ramachandran	Favored: 96.3%	Favored: 98.1%	Favored: 96.6%	Favored: 96.6%	Favored: 89.6%
Plot	Allowed: 3.7%	Allowed: 1.8%	Allowed: 3.3%	Allowed: 3.3%	Allowed: 9.4%
	Outliers: 0.0%	Outliers: 0.1%	Outliers: 0.1%	Outliers: 0.1%	Outliers: 1.0%

RF, reflection. $R_{sym} = \sum_h \sum_i |I_{h,i} - I_h| / \sum_h \sum_i I_{h,i}$, where I_h is the mean intensity of the i obervations of symmetry related reflections of h. $R = \sum |F_{obs} - F_{calc}| / \sum F_{obs}$, where $F_{obs} = F_P$, and F_{calc} is the calculated protein structure factor from the atomic model. R.m.s.d. in bond lengths and angles are the deviations from ideal values.